ACCSCIENCE PUBLISHING

Innovative Medicines & Omics

ORIGINAL RESEARCH ARTICLE

In silico evaluation of ursodeoxycholic acid from *Janja rubens* and its analogs as potential anti-Alzheimer's agents

Oluwafemi S. Aina[1,2*], Owoyemi W. Elegbeleye[3], Nafisat O. Babamusa[1], Mujeeb O. Rofiu[1], Kafayat A. Owoseni-Fagbenro[1], Olubusayo F. Semire[1], Olasupo A. Idris[1], Luqman A. Adams[1], and Oluwole B. Familoni[1]

[1]Department of Chemistry, Faculty of Science, University of Lagos, Lagos, Nigeria

[2]Department of Biological Sciences, Faculty of Basic Medical and Applied Sciences, Trinity University, Lagos, Nigeria

[3]Department of Marine Sciences, Faculty of Science, University of Lagos, Lagos, Nigeria

(This article belongs to the *Special Issue: Alzheimer's Disease and Other Forms of Dementias - Current Research Progress and Drug Development*)

Abstract

Alzheimer's disease (AD), one of the neurodegenerative disorders, is marked by the gradual degeneration of nerve cells in the brain or peripheral nervous system, along with abnormal protein aggregation. While significant efforts have been made to manage AD, a dearth of data remains on candidate phytochemicals and analogs in its treatment. Herein, we present alkaloids derived from the marine algae *Janja rubens* as potential inhibitors of human acetylcholinesterase (AChE) relevant to AD therapy. Using *in silico* tools, such as Protox II and SwissADME, 40 isolates were screened for toxicity and absorption, distribution, metabolism, and excretion properties. Molecular docking simulations were performed using PyRx 0.8, AutoDock Vina Wizard, and Discovery Studio 2020. A 50-nanosecond molecular dynamics simulation was performed using the Groningen Molecular Simulation in the LINUX environment and bio-organic molecules force field simulation (CHARMM 36). Ursodeoxycholic acid (AL20), an isolate from *J. rubens*, exhibited strong inhibitory activity against AChE with a binding energy of −8.5 kcal/mol, surpassing standard anti-Alzheimer drugs donepezil (−8.3 kcal/mol), galantamine (−7.7 kcal/mol), and rivastigmine (−6.4 kcal/mol). However, *in silico* data revealed a 73% probability of hepatotoxicity for AL20. Thereafter, seven derivatives (AL20A–G) were designed to improve properties for drug likeness. The amide analog, AL20E, showed superior inhibitory activity (−9.0 kcal/mol) and non-toxicity compared to AL20 and the standard drugs. This derivative also demonstrated strong interactions with the AChE enzyme, forming three hydrogen bonds with amino acid residues Pro290, Ser293, and Leu289. The brain or intestinal estimated permeation model predicted favorable gastrointestinal absorption and blood–brain barrier penetration for AL20E, indicating its potential as a central nervous system-active drug. Density functional theory and molecular dynamics analyses confirmed the chemical stability of AL20E, making it a promising candidate for the development of an anti-Alzheimer drug. This study highlights AL20E ([4R]-4-[{3S,7S,8R,9S,10S,13R,14S,17R}-3,7-dihydroxy-10,13-dimethylhexadecahydro-1H cyclopenta{a}phenanthren-17-yl]pentanamide) as a non-toxic, AchE inhibitor with enhanced drug-likeness. This study thereby presents AL20E for consideration as a lead compound in the development of novel Alzheimer's therapeutics.

Keywords: *Janja rubens*; *In silico* analysis; Ursodeoxycholic acid; Acetylcholinesterase; Anti-Alzheimer drug

***Corresponding author:**
Oluwafemi S. Aina
(oluwafemi.aina@trinityuniversity.edu.ng)

Citation: Aina OS, Elegbeleye OW, Babamusa NO, *et al. In silico* evaluation of ursodeoxycholic acid from *Janja rubens* and its analogs as potential anti-Alzheimer's agents. *Innov Med Omics*. 2025;2(4):74-92. doi: 10.36922/IMO025260027

Received: June 24, 2025

Revised: August 25, 2025

Accepted: September 2, 2025

Published online: October 14, 2025

1. Introduction

Neurodegenerative diseases, especially Alzheimer's disease (AD) and Parkinson's disease, are leading causes of death worldwide and are identified by a progressive loss of specific neuronal cell populations due to abnormal protein aggregation within neurons. AD is the most common cause of dementia in people over 65 years, affecting 55 million people and increasing at an alarming rate of 10 million cases/year worldwide.[1,2] Based on the cholinergic hypothesis of the pathogenesis of AD, the clinical features of dementia observed in this disease are ascribed to decreased levels of acetylcholinesterase (AChE), a neurotransmitter involved in memory and learning, in the hippocampus and cortex.[3] Notably, Food and Drug Administration (FDA)-approved drugs (donepezil, galantamine, memantine, and rivastigmine) only temporarily improve symptoms by increasing the number of neurotransmitters in the brain.

Ursodeoxycholic acid prevents the degradation of inhibitor of kappa B alpha, thereby leading to the inhibition of nuclear factor kappa B-dependent gene expression in microglia. The expression of these genes is associated with inflammation, a significant factor in neurodegenerative diseases, such as AD.[4] AChE inhibitors are commonly employed to partially alleviate symptoms in mild to moderate AD. They are also used to manage various other forms of dementia and central nervous system disorders, including Parkinson's disease, Lewy body-related dementia, mild cognitive impairment, Down syndrome, Korsakov disease, and vascular dementia.[5]

Researchers are currently actively designing, synthesizing, and evaluating new bioactive compounds for Alzheimer's treatment with minimal side effects.[6] For instance, ursodeoxycholic acid has been found to reduce neuronal loss in prion-infected cerebellar slice cultures.[7] In addition, in models of acute bilirubin encephalopathy, ursodeoxycholic acid treatment has been demonstrated to prevent apoptosis induced by unconjugated bilirubin in astrocytes and fetal neurons isolated from rats.[8] Alkaloids of marine algae are rare and mostly belong to the indole and phenylethylamine groups. In addition, the biological properties of these alkaloids remain under investigation.[9,10] While current treatments for neurodegenerative diseases exist, a critical gap remains in the availability of diverse, non-toxic, and highly effective phytochemical and synthetic drug candidates discoverable through a rapid and cost-effective computational approach. Therefore, this study aims to develop a potent, non-toxic, and anti-neurodegenerative compound from *Jania rubens* alkaloids, specifically by optimizing ursodeoxycholic acid derivatives using a multi-stage *in silico* methodology to identify a potential lead compound with a favorable toxicity profile and enhanced drug-likeness.

2. Materials and methods

2.1. Isolates from red seaweed *Jania rubens*

Phytochemicals were extracted and analyzed from the red seaweed *J. rubens* as described by El-Din and El-Ahwany.[11] The chemical names and structures of the 40 isolates investigated herein are presented in Table 1 and Figure 1, respectively.

2.2. Toxicity analysis of phytochemicals from *Jania rubens*

The target phytochemicals were screened for toxicity by screening using the Protox II web server (https://tox.charite.de/protox3/). We generated the Simplified Molecular Input Line Entry System (SMILES) representation of each phytochemical compound from *J. rubens* drawn using ChemDraw (Version 14.0, PerkinElmer Informatics, United States of America) and saved it in.sdf format on the server. The retrieved toxicity information included hepatotoxicity, carcinogenicity, immunotoxicity, mutagenicity, and cytotoxicity.

2.3. Preparation of enzymes and docking study

Protein structures used were initially cleaned by removing all solvent molecules and the co-crystallized ligands before docking. Molecular docking calculations for the 40 compounds against the Alzheimer protein, AChE (PDB ID: 4EY6), were undertaken using PyRx (Version 0.8, The Scripps Research Institute, United States of America) and Discovery Studio (Version 2020, BIOVIA, France), with a sphere (15 Å radius) that can accommodate the cavity centered on the binding sites of the protein structure. This approach ensured alignment in their conformations.[12] Standard protonation states of the protein based on neutral pH were used in the docking studies. The isolated structures were built using ChemDraw. Variable orientations of each ligand were searched and ranked based on their re-rank score. For each docking simulation, the maximum number of iterations for the docking algorithm was set to 9, with a maximum population size of 9 mode runs per ligand. The root mean square deviation (RMSD) threshold for multiple poses was set to 1.00 Å.[13]

2.4. Structural modification of lead compound AL20

Compound AL20, as the lead candidate with the highest binding energy of −8.5 kcal/mol, was selected for derivatization due to unfavorable toxicity profiles. Consequently, seven hypothetical compounds (AL20A–AL20G) were generated using ChemDraw. The structures were saved in the.sdf format, and their corresponding

Table 1. Structural information of phytochemicals (AL1–AL40) investigated from red seaweed *Jania rubens*[11]

Compound	Chemical name	Molecular formula	Molecular weight (g/mol)
AL1	2-Imidazolidinone	$C_3H_6N_2O$	86.0940
AL2	2-Cyclohexylpiperidine	$C_{11}H_{21}N$	167.2960
AL3	Methylene chloride	CH_2C_{l2}	84.9270
AL4	6-Methyl-4-([4-methylphenyl] sulfonyl)-5-heptenoic acid	$C_{15}H_{20}O_4S$	296.3810
AL5	3-(3-Hydroxybutyl)-2,4,4trimethyl-2-cyclohexen-1-one	$C_{13}H_{22}O_2$	210.3170
AL6	3-Ethyl-5-(2-ethylbutyl)-octadecane	$C_{26}H_{54}$	366.7180
AL7	Heptadecane	$C_{17}H_{36}$	240.4750
AL8	Hexadecanal	$C_{16}H_{32}O$	240.4310
AL9	Tetradecanoic acid	$C_{14}H_{28}O_2$	228.3760
AL10	9-hexadecenoic acid	$C_{16}H_{30}O_2$	254.4140
AL11	Pentadecanoic acid	$C_{15}H_{30}O_2$	242.4030
AL12	3,7,11,15-Tetramethyl-2-hexadecen-1-ol	$C_{20}H_{40}O$	296.5390
AL13	6,10,14-Trimethyl-2-pentadecanone	$C_{18}H_{36}O$	268.4850
AL14	Pentadecanal	$C_{15}H_{30}O$	226.4040
AL15	3-Eicosyne	$C_{20}H_{38}$	278.5240
AL16	Hexadecenoic acid	$C_{16}H_{30}O_2$	254.4140
AL17	9-Oximino-2,7-diethoxyfluorene	$C_{17}H_{17}NO_3$	283.3270
AL18	Hexadecanoic acid methyl ester	$C_{17}H_{34}O_2$	270.4570
AL19	L-(+)-Ascorbic acid 2,6-dihexadecanoate	$C_{38}H_{68}O_8$	652.9540
AL20	Ursodeoxycholic acid	$C_{24}H_{40}O_4$	392.5800
AL21	Methyl 13-octadecenoate	$C_{19}H_{36}O_2$	296.4950
AL22	Phytol	$C_{20}H_{40}O$	296.5390
AL23	Trans-13-octadecenoic acid	$C_{18}H_{34}O_2$	282.4680
AL24	Octadecanoic acid	$C_{18}H_{36}O_2$	284.4840
AL25	Heptasiloxane	$H_{16}O_6Si_7$	308.7170
AL26	Octanoic acid	$C_8H_{16}O_2$	144.2140
AL27	Octasiloxane	$H_{18}O_7Si_8$	354.8170
AL28	Squalene	$C_{30}H_{50}$	410.7300
AL29	9,12,15-Octadecatrienoic acid	$C_{18}H_{30}O_2$	278.4360
AL30	Oleic acid	$C_{18}H_{34}O_2$	282.4680
AL31	17-Pentatriacontene	$C_{35}H_{70}$	490.9450
AL32	Propanoic acid	$C_3H_6O_2$	74.0790
AL33	Rhodopsin	$C_{40}H_{58}O$	554.9030
AL34	Stigmasterol	$C_{29}H_{52}O$	416.7340
AL35	Withaferin A	$C_{28}H_{38}O_6$	470.6060
AL36	Cholest-5-en-3-one	$C_{27}H_{44}O$	384.6480
AL37	Cyclopropanebutanoic acid	$C_7H_{12}O_2$	128.0837
AL38	Pregn-5-ene-3,20-dione	$C_{21}H_{30}O_2$	314.4690
AL39	2,4,6-Decatrienoic acid	$C_{10}H_{14}O_2$	166.2200
AL40	Demecolcine	$C_{21}H_{25}NO_5$	371.4330

SMILES notations were uploaded onto the Protox II web server as outlined in Section 2.2 to evaluate their toxicity profiles against necessary compliance with drug-likeness rules.[14]

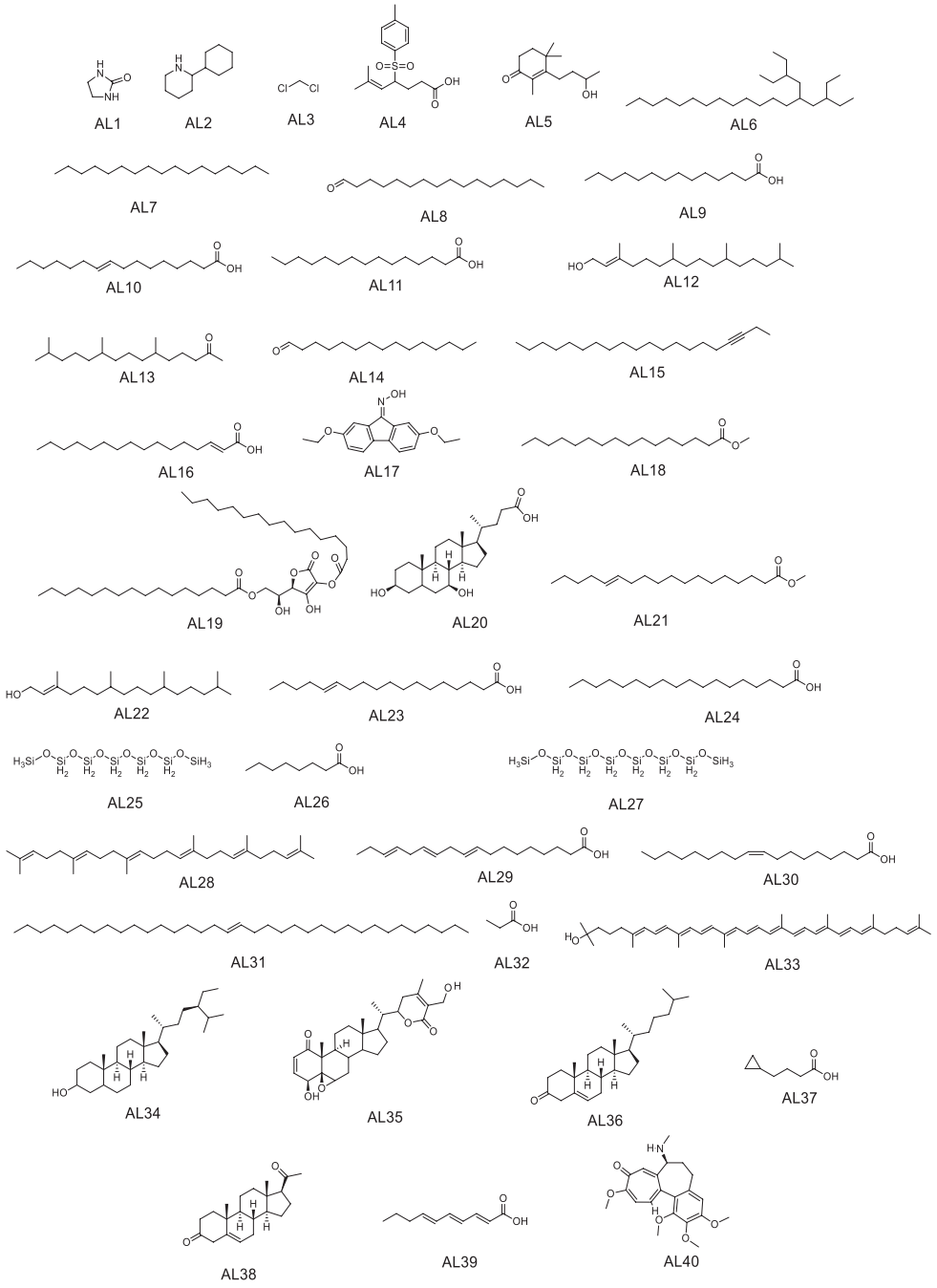

Figure 1. Molecular structures of isolated compounds from red seaweed *Jania rubens*

2.5. Drug-likeness and bioactivity

The seven derivative test compounds (AL20A–AL20G) were investigated using their SMILES representations on the admetSAR2 web server (lmmd.ecust.edu.cn/admetsar2) to predict absorption, distribution, metabolism, and excretion (ADME) parameters. Furthermore, bioactivity assessment using the Molinspiration web server was conducted to determine their potential as candidates for further drug development. Gastrointestinal (GI) and blood–brain barrier characteristics (brain or intestinal estimated permeation method [BOILED-Egg]) of the top three lead compounds obtained from AL20 were also obtained and analyzed.

2.6. Density functional theory studies

The geometry optimization of the lead AL20 and the top three derivative compounds, AL20B, AL20D, and AL20E, was carried out using the Gaussian 09W (Gaussian, Inc., United States of America) program.[15] Becke's three-parameter hybrid model with the Lee, Yang, and Parr's (B3LYP) correlation functional[16] was employed in combination with the Pople's standard, split-valence triple-zeta basis set (6–311++G[d,p])[17] for the calculations of density functional theory (DFT). The investigation of each compound's structural electronic data, chemical reactivity, molecular electrostatic potential map, molecular atomic charges, and molecular orbital properties was conducted. The simulated results were analyzed using GaussView software (Version 6.0, Gaussian, Inc., United States of America).[18]

2.7. Molecular dynamics simulation by Groningen Molecular Simulation

The molecular dynamics (MD) simulations of the lead compounds (AL20, AL20E) and reference drug (donepezil) were investigated against AChE, assessing protein (flexible)–ligand interactions stability and flexibility during binding.[19] Groningen Molecular Simulation (GROMACS) via the LINUX environment was employed to simulate the conformations, and the CHARMM 36 force field was used to generate the topological data for the complex. Small molecule topology and coordinate information were obtained from the CHARMM general force field (https://cgenff.com/). The macromolecular system was solvated in an aqueous phase using the simple point charge-216 water model and neutralized using a 0.15 M sodium chloride solution. A dodecahedron box was used to encapsulate the system, and 5,000 iterations of the steepest descent strategy were used to minimize energy. The equilibrium of ion molecules around the macromolecule was achieved at 310 K and 1.0 bar using the setup of constant number of particles, system pressure, and temperature, as well as constant number of particles, system volume, and temperature. A 50-nanosecond MD simulation was performed to generate structural trajectories for the analysis. Key parameters assessed include the RMSD, the root mean-square fluctuation (RMSF), the solvent-accessible surface area (SASA), hydrogen bonds (HBs), and the radius of gyration (Rg).

3. Results and Discussions

3.1. Toxicity analysis, druglikeness, and binding energy of lead phytochemicals from *Janiа rubens*

Toxicity evaluation is crucial in the identification and development of drugs. Lead compounds from *J. rubens* investigated using the Protox II web server are presented in Table 2. The toxicity profiles of the reference drugs are shown in Table 3. The summary of their binding energies is given in Table 4.

The isolated AL20 (ursodeoxycholic acid), alongside seven others, has exhibited high inhibitory activity against the human AChE protein (4EY6) crystal (Figure 2). The three standard reference drugs considered in this study are also included in Figure 2.

Druglikeness of five isolates with the good binding energy was analyzed using the SwissADME web server (http://www.swissadme.ch/index.php) and presented in Figure 3. Their compliance (or non-violation) with standard drug-likeness rules is presented in Table 5.

Out of the 40 isolates investigated, seven (AL1, AL4, AL5, AL26, AL32, AL37, and AL39) are non-toxic relative to the reference standard drugs (Table 3), whereas isolates AL17, AL20, AL35, AL38, and AL40 (Table 2) flouted one or more toxicity limitations. Interestingly, the isolates AL20, AL36, AL17, and AL35 demonstrated superior performance as anti-Alzheimer drug candidates based on their binding energy against human AChE enzyme (4EY6) (Table 4) compared to donepezil, galantamine, and rivastigmine (anti-Alzheimer standard drugs). Isolate AL20 (ursodeoxycholic acid) was therefore selected as the target moiety for further investigation through derivatization (Figure 4).

The isolate AL20 (ursodeoxycholic acid) exhibited the highest inhibitory activity against the human AChE

Table 2. Toxicity profiles of the *Janiа rubens* lead compounds

Toxicity profiles	Prediction (probability)											
	AL1	AL4	AL5	AL17	AL20	AL26	AL32	AL35	AL37	AL38	AL39	AL40
Hepatotoxicity	No (0.85)	No (0.54)	No (0.61)	No (0.64)	Yes (0.73)	No (0.52)	No (0.69)	No (0.93)	No (0.59)	No (0.67)	No (0.59)	No (0.68)
Carcinogenicity	No (0.88)	No (0.75)	No (0.68)	Yes (0.56)	No (0.79)	No (0.63)	No (0.76)	No (0.55)	No (0.66)	Yes (0.56)	No (0.69)	No (0.59)
Immunotoxicity	No (0.99)	No (0.99)	No (0.99)	No (0.72)	No (0.78)	No (0.99)	No (0.99)	Yes (0.99)	No (0.99)	Yes (0.96)	No (0.99)	Yes (0.99)
Mutagenicity	No (0.52)	No (0.68)	No (0.61)	Yes (0.59)	No (0.56)	No (100)	No (0.93)	No (0.79)	No (0.72)	No (0.99)	No (0.68)	No (0.87)
Cytotoxicity	No (0.80)	No (0.71)	No (0.95)	No (0.74)	No (0.76)	No (0.74)	No (0.75)	Yes (0.87)	No (0.76)	No (0.79)	No (0.75)	Yes (0.66)

Table 3. Toxicity compliance of standard drugs for Alzheimer's disease

Target	Prediction (probability)		
	Donepezil	Galantamine	Rivastigmine
Hepatotoxicity	No (0.98)	No (0.93)	No (0.93)
Carcinogenicity	Yes (0.50)	No (0.65)	No (0.74)
Immunotoxicity	Yes (0.95)	Yes (0.98)	Yes (0.69)
Mutagenicity	No (0.53)	No (0.76)	No (0.70)
Cytotoxicity	Yes (0.63)	Yes (0.50)	No (0.66)

Table 4. Complex binding scores of human acetylcholinesterase (4EY6) isolate from *Jania rubens*

4EY6-isolate complex	Binding energy
4EY6_AL20	−8.5
4EY6_AL36	−8.4
4EY6_AL17	−8.3
4EY6_AL35	−8.3
4EY6_donepezil	−8.3
4EY6_AL28	−8.1
4EY6_AL38	−8.1
4EY6_AL40	−8.0
4EY6_galantamine	−7.7
4EY6_AL34	−7.3
4EY6_AL39	−7.1
4EY6_AL4	−6.9
4EY6_rivastigmine	−6.4
4EY6_AL26	−5.7
4EY6_AL5	−5.5
4EY6_AL37	−5.3
4EY6_AL1	−4.0
4EY6_AL32	−3.7

protein crystal (4EY6), as presented in Table 4, along with other high-binding bioactive isolates. The three standard reference drugs considered in this study are shown in Figure 4. The drug-likeness of the high-binding energy isolates was analyzed using the SwissADME web server (http://www.swissadme.ch/index.php). We observed that five of the isolates (AL17, AL20, AL35, AL38, and AL40) fall within the optimal physicochemical space for bioavailability. All five isolates exhibited high GI absorption capability, while AL17, AL38, and AL40 showed blood–brain barrier permeability (Table 5). However, isolated AL35 violated one of the Ghose rules, suggestive of poor oral bioavailability.

3.2. Toxicity probability and bioavailability of the derivatives of AL20 (the highest binding isolate)

Despite its strong AChE inhibition and favorable drug-likeness, isolate AL20 exhibited high hepatotoxicity (73%), prompting the desire for new derivatives of the moiety. Guided by structure-activity relationship principles, seven new derivatives of AL20 (AL20A, AL20B, AL20C, AL20D, AL20E, AL20F, AL20G) were designed to reduce the toxicity properties. AL20 was modified at the carboxylic functional group to carry a methyl group (AL20A), ketone (AL20B), aldehyde (AL20G), acid chloride (AL20C), amides (AL20E), and ester (AL20F). In addition, the butanoic acid side chain was removed, and one of the hydroxyl groups was hypothetically oxidized to a ketone (AL20D). These modifications aimed to improve their biocompatibilities. Figure 5 presents the structures of the new derivatives, while Table 6 shows their toxicity compliance investigated using the Protox 3 web server. Figure 4 depicts the bioavailability of the three best derivatives compared to the standard drug for AD.

Virtual toxicity screening of AL20 derivatives using the Protox II web server showed that AL20B, AL20D, and AL20E (Table 6) were non-toxic, unlike AL20C, AL20F, and AL20G, which showed a high probability of being hepatotoxic (57–63%), while AL20A and AL20G exhibited a probability of 60–69% of being immunotoxic. Notably, the non-toxic derivatives of AL20 isolate were more biocompatible than the standard Alzheimer's drugs, which displayed varying degrees of toxicity, including carcinogenicity, immunogenicity, and cytotoxicity (Table 3). Donepezil, galantamine, and rivastigmine are prescription drugs used in early- to mid-stage AD. However, their inherent toxicity remains a concern. Interestingly, the bioavailability results (Figure 4) of all AL20 non-toxic derivatives (AL20B, AL20D, and AL20E) showed superior drug-likeness properties compared to the three standard drugs. Thus, the non-toxic derivatives were subjected to further analysis.

3.3. Bioactivity score of lead derivatives

The bioactivity scores of the three best lead derivatives, AL20B, AL20D, and AL20E, the isolate AL20, and the reference drug donepezil are presented in Figure 6. The bioactivity scores were evaluated using several parameters, including G-protein-coupled receptor (GPCR) ligands, ion channel modulators, kinase inhibitors, nuclear receptor ligands, protease inhibitors, and enzyme inhibitors.

Compounds with bioactivity scores higher than 0.00 are defined as active, those between −0.50 and 0.0 are

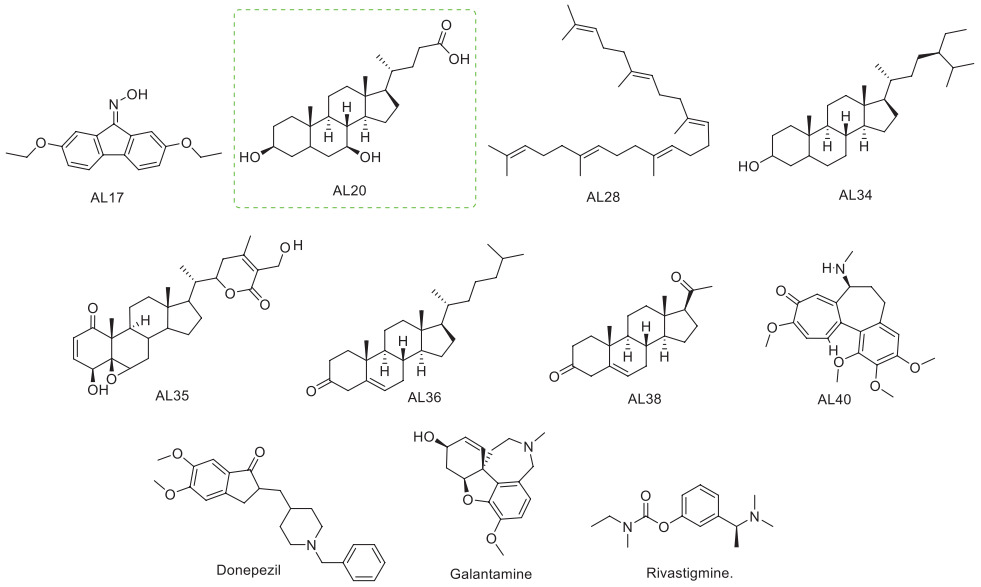

Figure 2. Structures of lead compounds of *Jania rubens* against human acetylcholinesterase and commonly used Alzheimer's drugs, donepezil, galantamine, and rivastigmine

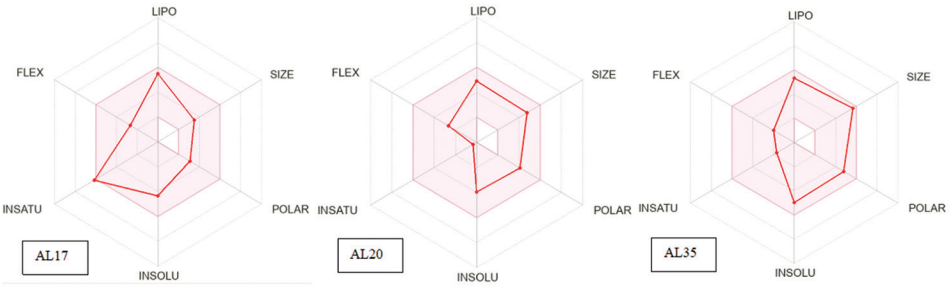

Figure 3. Lead compounds AL17, AL20, and AL35 with excellent binding energy and bioavailability (compliant physicochemical space)
Abbreviations: FLEX: Flexibility; INSATU: Saturation; INSOLU: Solubility; LIPO: Lipophilicity; POLAR: Polarity; SIZE: Molecular size.

Table 5. Compliance of active isolates with drug-likeness rules

Isolate	Lipinski	Ghose	Veber	Egan	Muegge	GI abs	BBB perm
AL17	0	0	0	0	0	High	Yes
AL20	0	0	0	0	0	High	No
AL35	0	1	0	0	0	High	No
AL38	0	0	0	0	0	High	Yes
AL40	0	0	0	0	0	High	Yes

Note: 0: No violation; 1: One violation.
Abbreviations: abs: Absorption; BBB: Blood–brain barrier; GI: Gastrointestinal; perm: Permeability.

moderately active, and scores below −0.50 are considered inactive.[20] They exhibited superior performance compared to donepezil in several bioactivity scores, including ion-channel modulator (0.2–0.4), protease inhibitor (0.1–0.4), enzyme inhibitor (0.6–0.8), nuclear receptor ligand (0.6–1.0), and GCPR ligands (0.0–0.4). However, derivatives AL20B and AL20D were inactive as kinase inhibitors (KI) (−0.8–−0.6).

3.4. Brain or intestinal estimated permeation model for blood–brain barrier permeability and GI absorption

The BOILED-Egg method predicts human GI absorption and blood–brain barrier (BBB) penetration using the SMILE string of the compounds. The algorithm utilizes two physicochemical models: lipophilicity (Wildman–Crippen LogP method [WLOGP]) and polarity (topological polar surface area), while estimating physicochemical descriptors, such as brain access and GI absorption for compounds AL20, AL20B, AL20D, and AL20E (Figure 7).

The analysis identifies the substrate of P-glycoproteins (PGP), which are detected as positive or negative in the BOILED-Egg method.[21,22] The statistical robustness, graphical nature, and speed of this method enable efficient

Figure 4. Bioavailability suitable physicochemical space of the standard drugs for Alzheimer's disease (donepezil, galantamine, and rivastigmine), AL20, and its lead derivatives (AL20B, AL20D, and AL20E)
Abbreviations: FLEX: Flexibility; INSATU: Saturation; INSOLU: Solubility; LIPO: Lipophilicity; POLAR: Polarity; SIZE: Molecular size.

Table 6. Toxicity compliance of AL20 designed derivatives, AL20A–AL20G

Target	Prediction (probability)							
	AL20	AL20A	AL20B	AL20C	AL20D	AL20E	AL20F	AL20G
Hepatotoxicity	Yes (0.73)	No (0.66)	No (0.63)	Yes (0.57)	No (0.53)	No (0.67)	Yes (0.62)	Yes (0.63)
Carcinogenicity	No (0.79)	No (0.80)	No (0.72)	No (0.66)	No (0.78)	No (0.63)	No (0.80)	No (0.72)
Immunotoxicity	No (0.78)	Yes (0.60)	No (0.83)	No (0.72)	No (0.53)	No (0.79)	No (0.53)	Yes (0.69)
Mutagenicity	No (0.56)	No (0.87)	No (0.78)	No (0.74)	No (0.94)	No (0.83)	No (0.63)	No (0.78)
Cytotoxicity	No (0.76)	No (0.89)	No (0.88)	No (0.77)	No (0.81)	No (0.74)	No (0.67)	No (0.88)

translation of molecular design in drug discovery and medicinal chemistry.[21] Drug-likeness models and methods, such as in-house physics-based LogP model, generalized born/surface area model, atom-additive method, WLOGP, Moriguchi LogP method, and Silicos-IT fragment- and topology-based model, as well as drug-likeness rules, such as Lipinski, Veber, Muegge, Ghost, and Egan, are incorporated in the BOILED-EGG tool. The SwissADME tool facilitates pharmacokinetics predictions, especially for ADME, bioavailability, and medicinal chemistry.[22,23]

More than 98% of small molecules are unable to cross the blood–brain barrier (BBB),[24] making the BBB an essential factor in the drug design process, particularly for central nervous system (CNS) disorders. The quantity of drug candidates absorbed by the intestinal system is a significant factor in assessing oral bioavailability,[25] thereby underlining the importance of the GI absorption of the molecules. PGP is a member of the ATP-binding cassette family (ABC) and an ABC transporter.[26] It acts as a biological barrier, pumping out toxins and xenobiotics

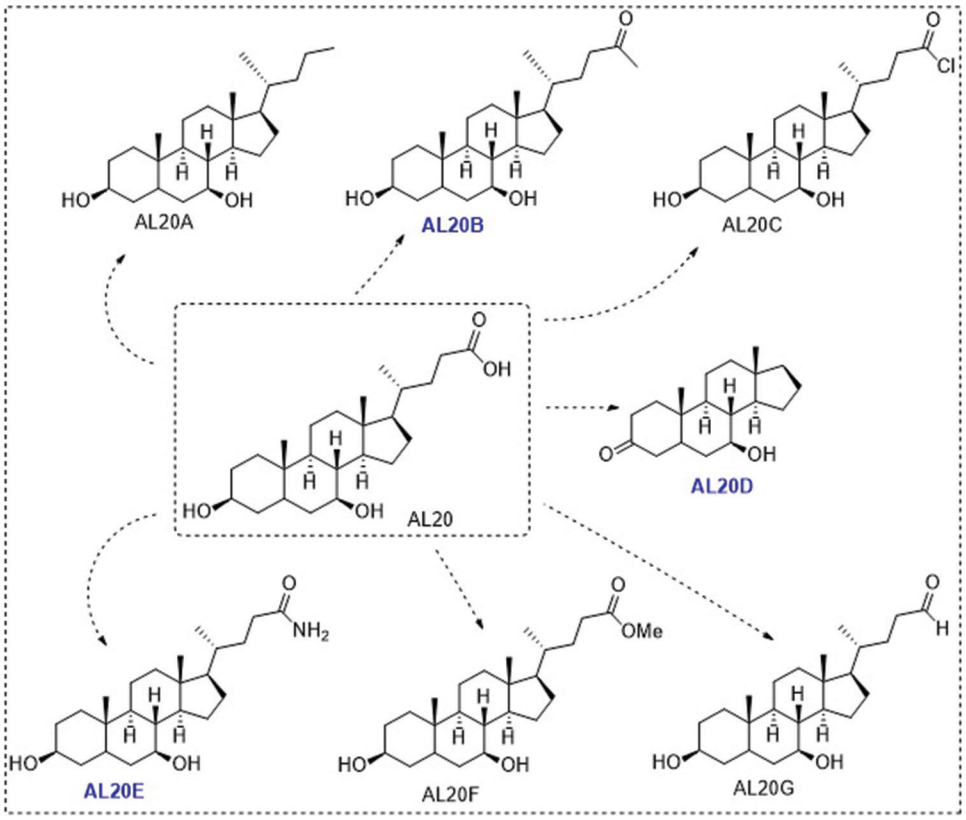

Figure 5. Structure of AL20 isolated from *Jania rubens* and its modified derivatives obtained through a structure-activity relationship study

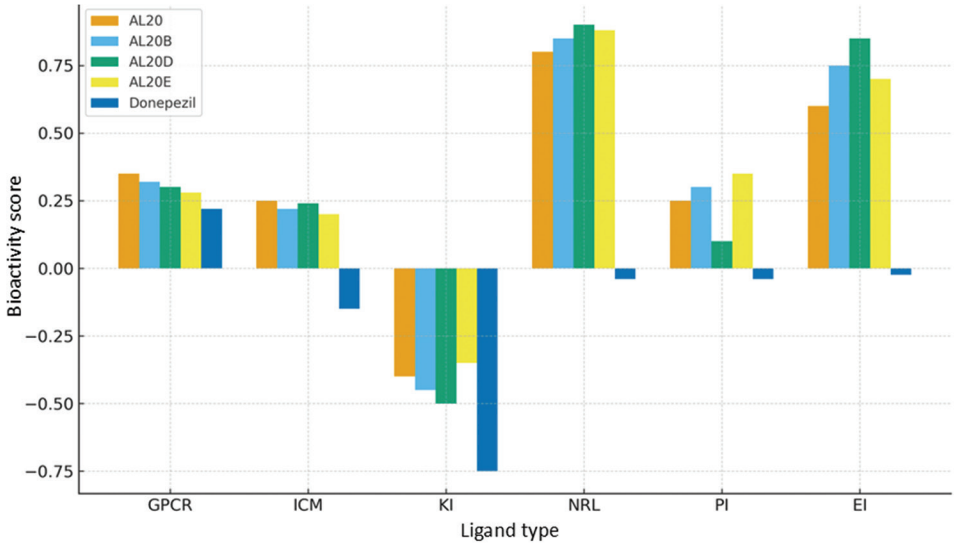

Figure 6. Bioactivity scores of *Jania rubens* phytochemical (AL20), its lead derivatives (AL20B, AL20D, and AL20E), and donepezil (Alzheimer reference drug)
Abbreviations: EI: Enzyme inhibitor; GPCR: G protein-coupled receptor ligand; ICM: Ion channel modulator; KI: Kinase inhibitor; NRL: Nuclear receptor ligand; PI: Protease inhibitor.

from cells while also contributing to the absorption of drugs.[27] The overexpression of ABC transporters causes multidrug resistance and is linked to the failure of disease treatments, such as cancer.[28]

The yellow region in Figure 7 represents a zone of compound having good permeation and absorption ability in both the BBB and GI. However, the white region defines good GI absorption but not BBB penetration. Molecules

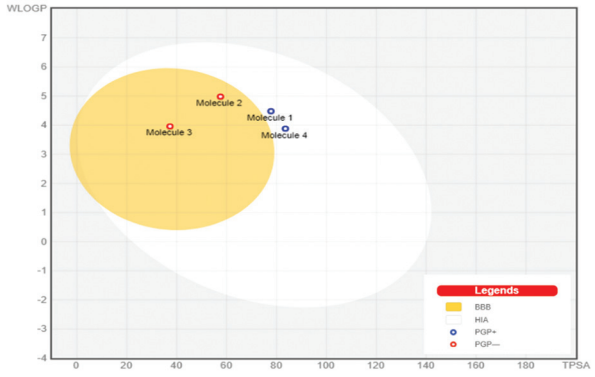

Figure 7. Brain or intestinal estimated permeation model of AL20 and its structurally modified non-toxic derivatives using the SwissADME web server (AL20, AL20B, AL20D, and AL20E are represented as molecules 1, 2, 3, and 4, respectively)
Abbreviations: BBB: Blood–brain barrier; HIA: Human intestinal absorption; PGP: P-glycoprotein; TPSA: Topological polar surface area; WLOGP: Wildman–Crippen LogP.

1 (AL20) and 4 (AL20E), marked with blue dots, and molecules 2 (AL20) and 3 (AL20D), marked with red dots, indicate that the former are predicted to be effluxed from the CNS by PGP, while the latter are predicted to escape PGP efflux. Notably, compounds expected to undergo PGP efflux still display good permeation and absorption ability. In contrast, compounds depicted in red dots (AL20 and AL20D), although they exhibit good permeation and absorption in the BBB, their CNS availability may still be negatively impacted by PGP.

3.5. Density functional theory measurements of target compounds

The molecular geometry optimization for the lead compound AL20's non-toxic derivatives (AL20B, AL20D, and AL20E) was performed using DFT/B3LYP level theory with 6–311+G (d,p) basis set. The optimized molecular geometry of the AL20s is shown in Figure 8, and the chemical reactivity parameters are listed in Table 7. The molecular electrostatic potential (MEP) map of AL20E is shown in Figure 9.

The chemical characteristics of the designed compounds AL20B, AL20D, and AL20E were analyzed using the highest occupied molecular orbital (HOMO) and lowest unoccupied molecular orbital (LUMO) energy levels.[29] This provides insights into the atomic orbital and electron density around the atomic surfaces to define the chemical stability in molecules based on the conceptual-DFT indices,[30] such as hardness, softness, electrophilicity index, and chemical potential. The global chemical hardness and softness measure the resistance and susceptibility of a molecule to exchange electrons with other molecules, respectively.[31] The electrophilicity index indicates the overall electrophilicity and nucleophilicity of a molecule. Furthermore, the feasibility of intermolecular electron transfer in the ground state is defined by the chemical potential.[32] The chemical reactivity descriptors were summarized in Table 7.

The band gaps of the designed compounds are in the increasing order of AL20D < AL20B < AL20E (Table 7). As shown by the frontier HOMO and LUMO molecular orbitals distribution (Figure 9), the carbonyl substituents likely enhanced the electrophilicity, leading to a lower energy gap as indicated in the smaller band gaps in AL20B and AL20D. The larger band gap in AL20E can be attributed to the amide substituent, which has a smaller electron-withdrawing effect compared to the carbonyl group. Compound AL20E also has the highest chemical potential (−0.136). The electrophilicity index value of 0.076 for AL20E demonstrates a stronger nucleophilic character compared to AL20B and AL20D, in the order of AL20D < AL20B < AL20E. AL20E utilizes the nature of conventional HBs with Ser293, Leu289, and Pro290 in interaction with the target receptor. Overall, it can be concluded that the designed compounds can be potential drug candidates for AD.

The MEP map provides information on molecular interactions and the chemical behavior of molecules with other molecular species.[33] The color gradient ranges from red (high electron density, negative electrostatic potential) to blue (low electron density, positive electrostatic potential), with green representing neutral regions. The MEP map for the AL20E derivatives was computed using DFT/B3LYP level of theory with 6–311++G (d,p) basis set (Figure 9). The red regions indicate sites for electrophilic attack, while the blue regions highlight areas susceptible to nucleophilic interactions. Consistent with the DFT-concept reactivity indices, the blue regions, such as the amino group in AL20E, align with nucleophilic interactions, supporting conventional HBs with Ser293, Leu289, and Pro290. In conclusion, the maps revealed possible surfaces of interactions between drugs and proteins.

The transition of electrons from HOMO to LUMO energy levels is represented by the electronic distribution on the HOMO and LUMO surfaces (Figure 9). It is inferred from the surfaces that the lower energy gaps for AL20D and AL20B may be well indicated by the localization of the electron density on the carbonyl or the aliphatic moiety, both in the HOMO and LUMO, after the transition. That is, the transition is occurring within the same regions or very close regions on the molecular surface. In AL20E, the transition from HOMO to LUMO will result in the transfer

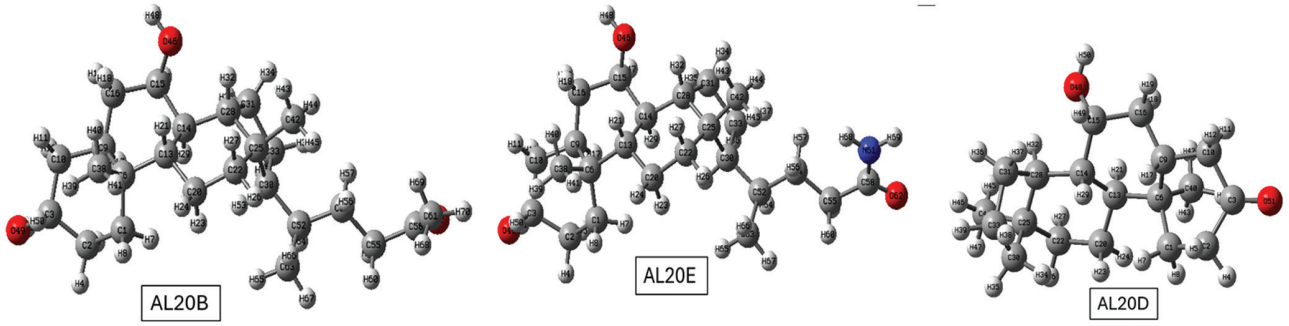

Figure 8. Geometry optimization of AL20 lead derivatives (AL20B, AL20D, and AL20E)

Table 7. Chemical reactivity parameters of the three AL20 lead derivatives

Derivatives	E_{HOMO}	E_{LUMO}	ΔE	IE	EA	H	S	ω	M
AL20B	−0.251	−0.026	0.225	0.251	0.026	0.1125	8.889	0.085	−0.139
AL20D	−0.248	−0.03	0.218	0.248	0.03	0.109	9.174	0.089	−0.139
AL20E	−0.256	−0.015	0.241	0.256	0.015	0.1205	8.299	0.076	−0.136

Abbreviations: ΔE: Energy gap; ω: Electrophilicity index; E_{HOMO}: Energy of the highest occupied molecular orbital; E_{LUMO}: Energy of the lowest unoccupied molecular orbital; EA: Electron affinity; H: Hardness; IE: Ionization energy; M: Chemical potential; S: Softness.

Table 8. Summary of docking results for AL20 hypothetical derivatives

Ligand	Binding affinity	RMSD/UB	RMSD/LB
4EY6_AL20E	−9.0	0	0
4EY6_AL20	−8.5	0	0
4EY6_donepezil	−8.3	0	0
4EY6_AL20B	−8.2	0	0
4EY6_AL20D	−8.1	0	0
4EY6_AL20C	−7.8	0	0
4EY6_AL20A	−7.8	0	0
4EY6_galantamine	−7.7	0	0
4EY6_AL20F	−7.6	0	0
4EY6_AL20G	−7.3	0	0
4EY6_rivastigmine	−6.4	0	0

Abbreviations: LB: Lower bound; RMSD: Root mean square deviation; UB: Upper bound.

of the electron distribution from the carbonyl or aliphatic region to the alicyclic region of the compound (Figure 9). This might explain the higher energy gap in the HOMO-LUMO transition.

3.6. Binding potentials of AL20 derivatives

It was necessary to dock the non-toxic derivatives of AL20 (AL20B, AL20D, and AL20E) to confirm their binding affinity (Table 8). Extracted three-dimensional (3D) structures of the interactions are presented in Figures 10-12.

It was necessary to dock these derivatives, expecting that any of those non-toxic derivatives would also provide excellent binding, and it was noteworthy that derivative AL20E performed better than phytochemical AL20 and all the reference drugs (Table 8) as a potential inhibitor of human AChE (4EY6), a significant target for therapeutic drugs.

The comparative analysis of AL20, AL20E, and donepezil binding to AChE (PDB: 4EY6) reveals distinct inhibitory mechanisms (Figures 11-13), despite all three ligands sharing a common anchor point: Trp_{286}. This residue is part of the peripheral anionic site (PAS) at the gorge entrance. In every complex, the ligand's aromatic core forms a stabilizing hydrophobic π–π stacking interaction with it. Beyond this initial binding, their strategies diverge the reference drug donepezil and the ligand AL20 primarily occupies the PAS, blocking the entrance. However, AL20 achieves a potentially more stable fit by utilizing an additional hydrogen bond with the polar residue Thr_{175}, differentiating its mechanism from the solely aromatic interactions of Donepezil.

The most unique binding profile belongs to AL20E (Figure 11), which acts as a deep-gorge binder. Its extended flexible aliphatic chain enables it to span the entire active site. While still anchored by Trp_{286} at the PAS, the ligand's tail reaches a deeper sub-site, forming a key hydrogen bond with Val_{340}. This strategy of dual-site occupancy is characteristic of potent inhibitors designed to maximize contact area, making AL20E's inhibitory mechanism the

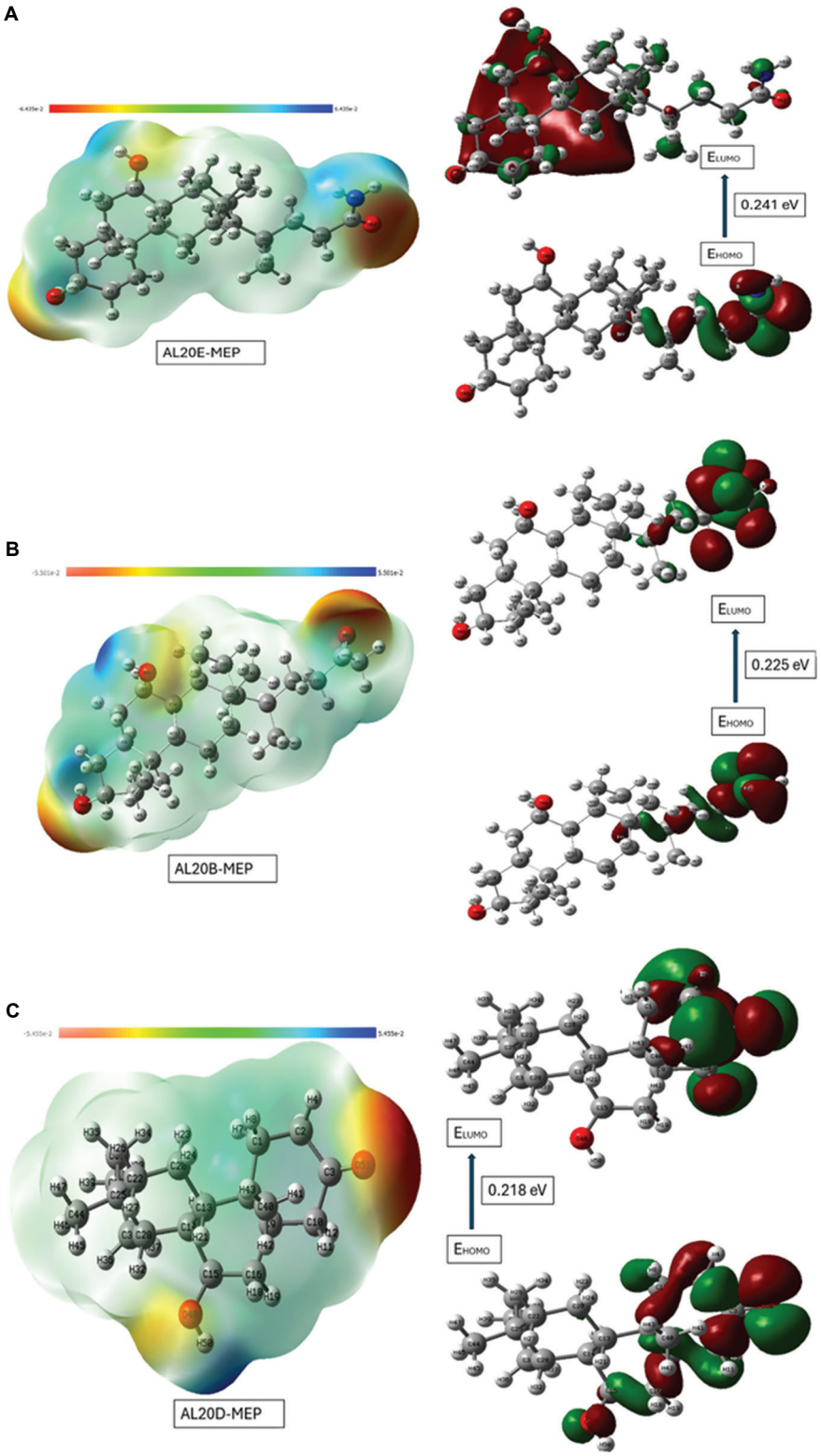

Figure 9. The MEP and HOMO–LUMO transitions of AL20 derivatives. (A) AL20E. (B) AL20B. (C) AL20D.
Abbreviations: E: Energy; HOMO: Highest occupied molecular orbital; LUMO: Lowest unoccupied molecular orbital; MEP: Molecular electrostatic potential.

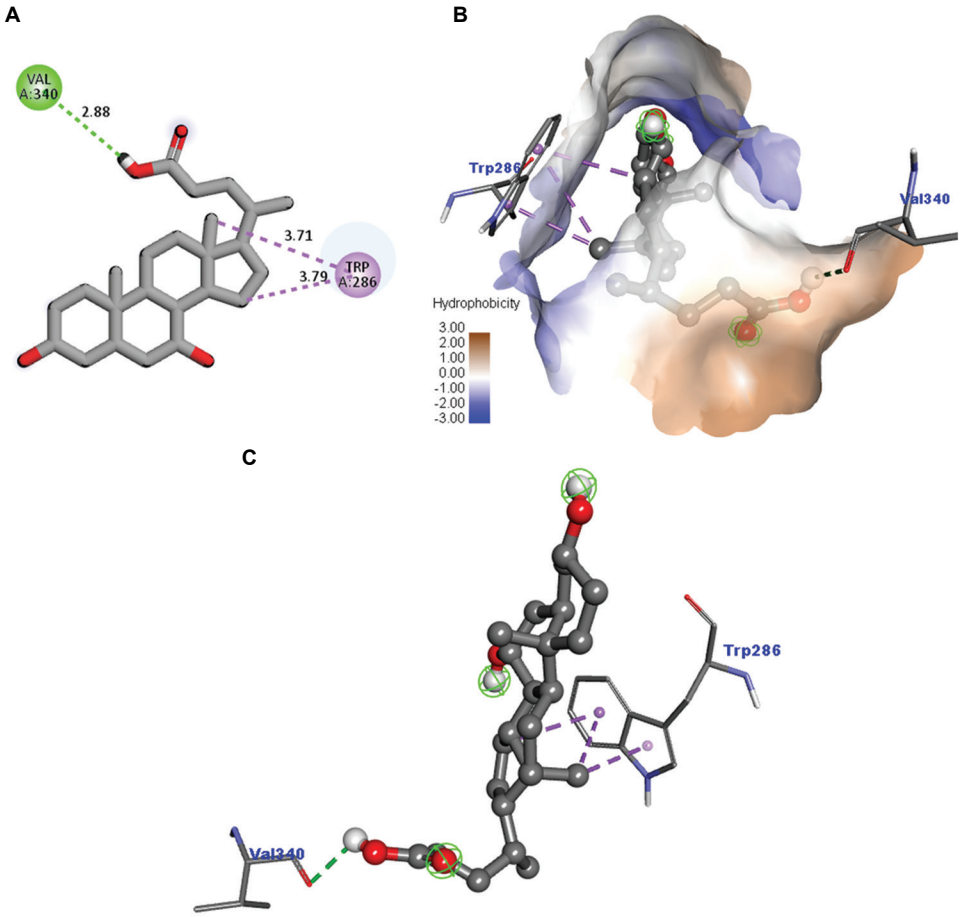

Figure 10. Two- and three-dimensional structures of the 4EY6_AL20 complex. (A) Bonding amino acids in a two-dimensional view. (B) Hydrophobic interactions. (C) Binding residues in a three-dimensional view.

most structurally complex and potentially more effective than AL20 and donepezil.

3.7. Molecular dynamics of lead derivatives and reference drug

The backbone of AChE (4EY6) and the RMSD values of 4EY6_AL20, 4EY6_AL20E, and 4EY6_donepezil complexes are shown in Figure 13, while the RMSF plot to determine the flexibility of each residue over a 50-nanosecond simulation is presented in Figure 14.

Figure 15 depicts the hydrogen bond plots for complexes 4EY6_AL20, 4EY6_AL20E, and 4EY6_donepezil measured in nanoseconds. The thermodynamic stability and energy profiles of 4EY6_AL20, 4EY6_AL20E, and 4EY6_donepezil complexes in terms of temperature, pressure, and density, with minimal fluctuations measured in picoseconds are presented in Figure 16. The SASA and Rg energy plots for complexes 4EY6_AL20, 4EY6_AL20E, and 4EY6_donepezil are illustrated in Figure 17.

Molecular dynamics simulations offer insights into the dynamic behavior of protein-ligand complexes, including structural stability, interaction strength, and thermodynamic properties.[34] In this molecular dynamics study, we compared the complexes formed from two non-toxic derivatives of AL20: 4EY6_AL20 and 4EY6_AL20E with the complex formed with the reference drug, 4EY6_donepezil. Donepezil was chosen to serve as a reference ligand due to its established efficacy as an AChE inhibitor.[35]

3.7.1. Stability analysis of the AChE_AL20 complex

The RMSD values of 4EY6_AL20, 4EY6_AL20E, and 4EY6_donepezil for the backbone of AChE (4EY6) were fluctuating between 0.12 and 0.24 nm, 0.10 and 0.18 nm, and 0.12 and 0.23 nm, with average RMSD values of 0.180 nm, 0.140 nm, and 0.175 nm, respectively. This indicated that the compound, AL20E, having the lowest RSMD value of 0.140 nm, is more stable across the 50-nanosecond simulations compared to AL20 and donepezil (Figure 13A).

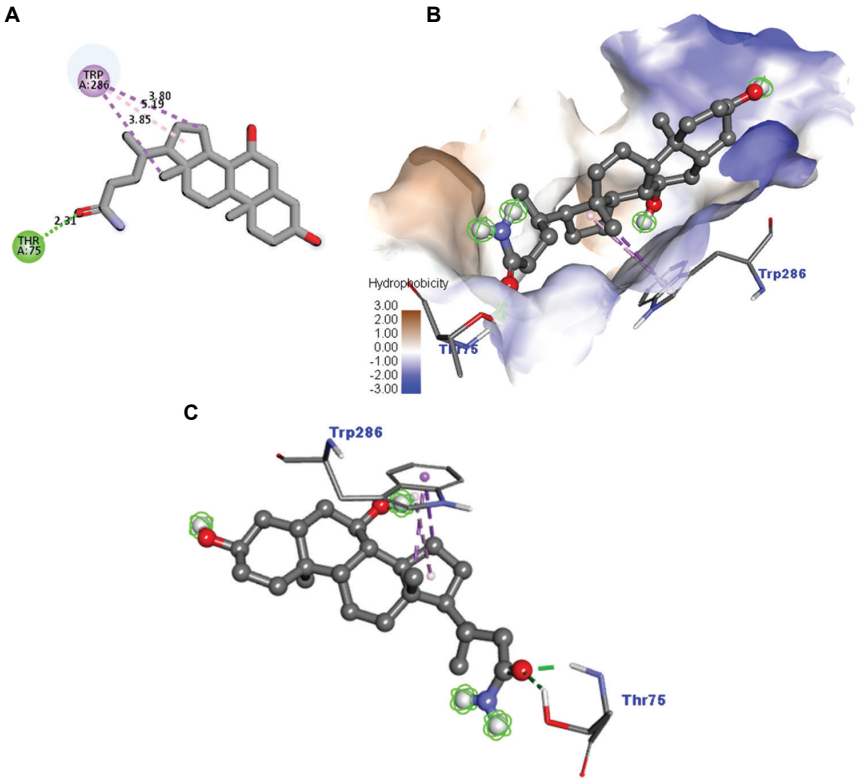

Figure 11. Two- and three-dimensional structures of 4EY6_AL20E complex. (A) Bonding amino acids in a two-dimensional view. (B) Hydrophobic interactions. (C) Binding residues in a three-dimensional view.

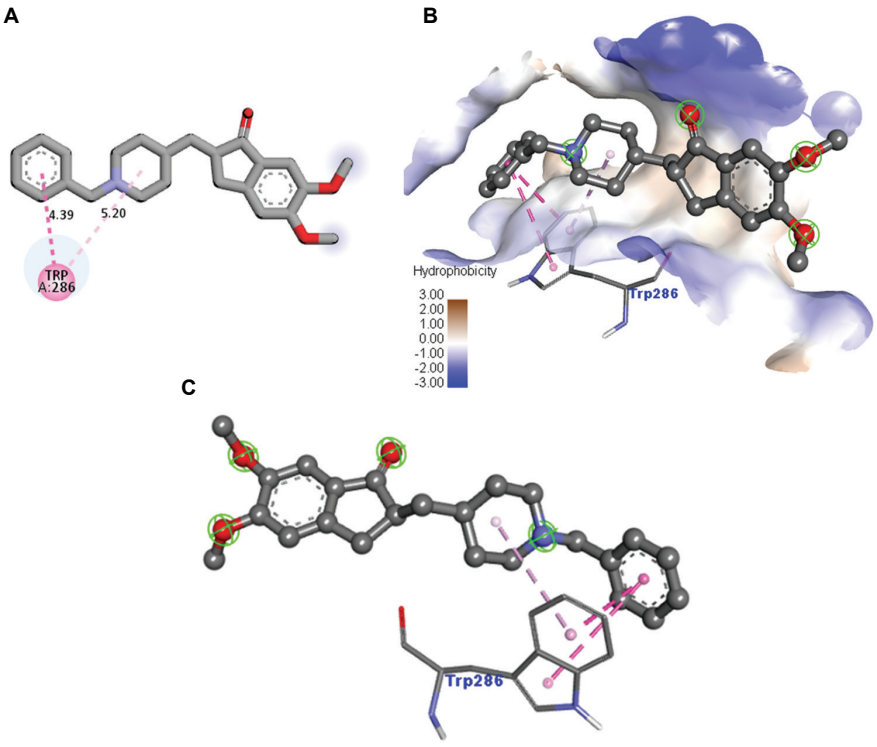

Figure 12. Two- and three-dimensional structures of 4EY6_donepezil complex. (A) Bonding amino acids in a two-dimensional view. (B) Hydrophobic interactions. (C) Binding residues in a three-dimensional view.

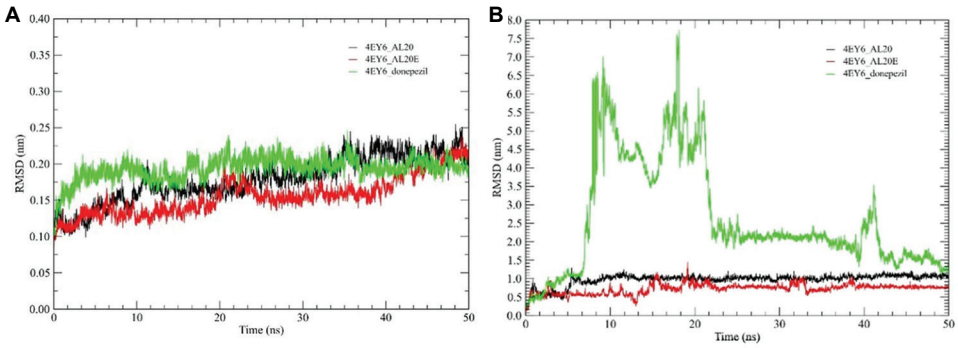

Figure 13. Root mean square deviation (RMSD) plots for complexes 4EY6_AL20, 4EY6_AL20E, and 4EY6_donepezil. (A) Backbone. (B) Ligand.

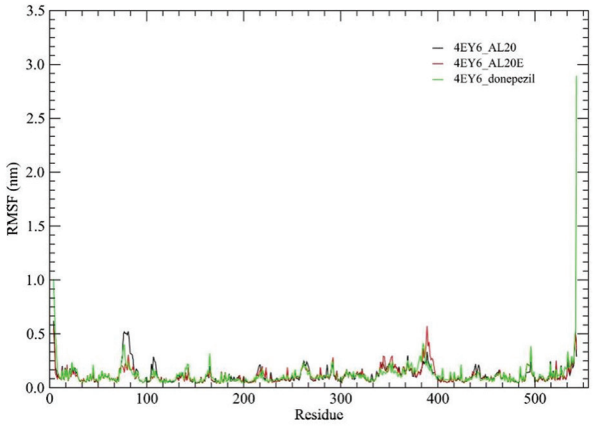

Figure 14. Root mean square fluctuation for complexes 4EY6_AL20, 4EY6_AL20E, and 4EY6_donepezil.

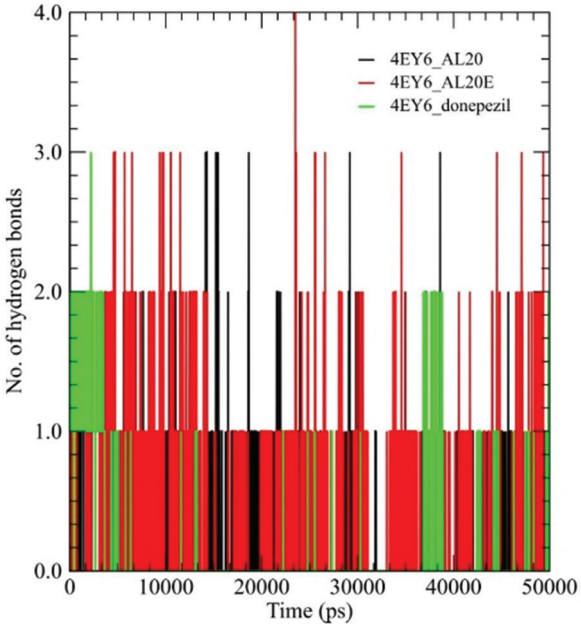

Figure 15. Stability analysis measured in nanoseconds for complexes 4EY6_AL20, 4EY6_AL20E, and 4EY6_donepezil.

The RMSD values of the ligands of AL20, AL20E, and donepezil were predicted, with AL20 starting at approximately 0.4 nm and fluctuating between 0.6 and 1.0 nm. Similarly, AL20E started at approximately 0.00 nm and fluctuated slightly between 0.5 and 0.8 nm. In contrast, donepezil started at approximately 0.2 nm but spiked drastically after 5 ns, showing multiple peaks at 6.0 to 7.5 nm, after which it stabilized to around 1.5 to 2.5 nm after 22 ns (Figure 13B). The average RMSD values of AL20, AL20E, and donepezil are 0.70 nm, 0.40 nm, and 3.85 nm, respectively. This indicates that AL20E binds the strongest to AChE as it exhibits the most stable interaction, as shown in Figure 13.

Hydrogen bonding analysis of the 4EY6_AL20 complex showed stable interactions, with 1–2 HBs throughout the simulation and a transient increase to 3 bonds at 15–18 ns (Figure 15). In comparison, 4EY6_AL20E exhibited stronger interactions, fluctuating between one and three HBs and peaking at four bonds around 20 ns. The reference complex, 4EY6_donepezil, showed the least fluctuation, maintaining 1–2 HBs with a single increase to 3 HBs at 2 ns. Overall, 4EY6_AL20E exhibited the highest and most consistent HB count, consistent with its strong binding capacity.

3.7.2. Flexibility analysis of the AChE_AL20 complex

The RMSF plot shows the flexibility of each residue over a 50-nanosecond simulation (Figure 14). 4EY6_AL20 fluctuated mostly below 0.5 nm, with a peak at residue 80 (0.5 nm), suggesting flexibility. Similarly, peaks of 4EY6_AL20E are minimal, with most residues below 0.4 nm, but exhibit a peak near residue 400 (0.5 nm), suggesting flexibility in that region. In contrast, 4EY6_donepezil fluctuates more than 4EY6_AL20 and 4EY6_AL20E, with a small peak near residue 400 (0.5 nm) and a large peak at the C-terminal (2.9 nm). The high fluctuation at the C-terminal of 4EY6_donepezil suggests flexibility or unfolding, making it the least stable, while 4EY6_AL20E is the most stable complex with the least fluctuation, as

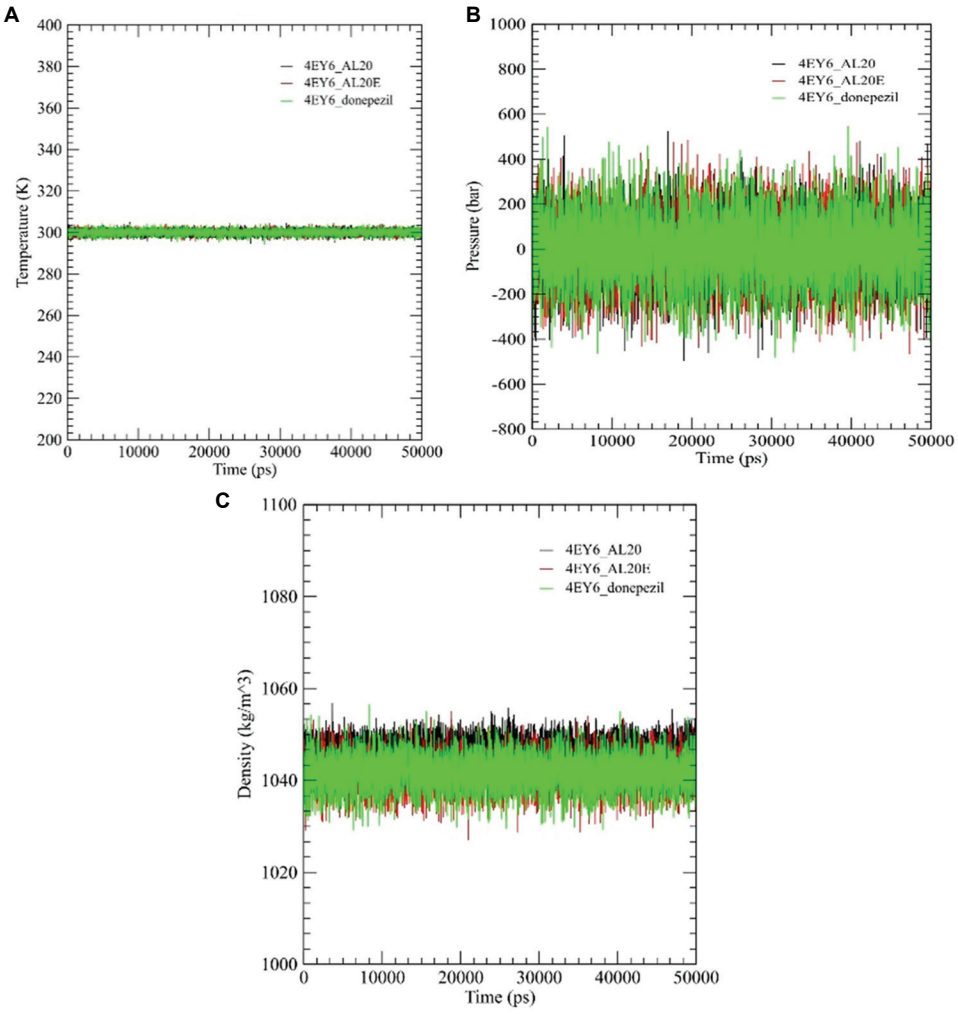

Figure 16. Gromacs energy measured in picoseconds for complexes 4EY6_AL20, 4EY6_AL20E, and 4EY6_donepezil. (A) Temperature. (B) Pressure. (C) Density.

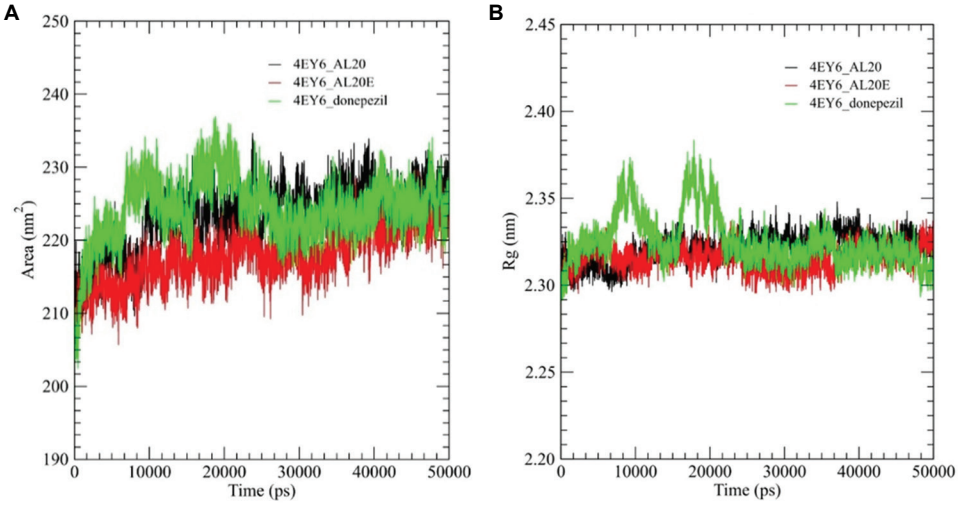

Figure 17. Structural flexibility and compactness measured in nanoseconds for complexes 4EY6_AL20, 4EY6_AL20E, and 4EY6_donepezil (A) Solvent-accessible surface area (B) Radius of gyration.

shown in Figure 14.

3.7.3. Compactness analysis of the AChE_AL20 complex

Radius of gyration value (Figure 17B) for both 4EY6_AL20 and 4EY6_AL20E ranged from 2.30 to 2.34 nm with minimal fluctuations. In contrast, 4EY6_donepezil started around 2.30 nm and exhibited significant fluctuations between 2.30 and 2.37 nm at around 10,000–20,000 ps (10–20 ns). The fluctuation stabilized toward the end of the simulation. 4EY6_AL20E displayed similar Rg values to 4EY6_AL20 but with slightly reduced fluctuations, suggesting improved structural integrity. In conclusion, 4EY6_AL20E is more compact and stable compared to 4EY6_AL20 and 4EY6_donepezil (Figure 17B).

Solvent accessible surface area reflects the extent of the protein's surface exposure to solvent. As shown in Figure 17, 4EY6_AL20 and 4EY6_AL20E showed a similar trend of fluctuating between 215 and 230 nm^2 and 210 and 225 nm^2, respectively. In contrast, 4EY6_donepezil increased from 202 nm^2 to 234 nm^2 for the first 20 ns and became stable for the rest of the simulation. Overall, 4EY6_AL20 and 4EY6_AL20E displayed relatively stable SASA values, whereas 4EY6_donepezil exhibited greater variation, suggesting higher solvent exposure and lower structural stability (Figure 17).

3.7.4. Thermodynamic stability and energy profiles of the AChE_AL20 complex

Regarding the Gromacs energies, the temperature (Figure 16A) of 4EY6_AL20, 4EY6_AL20E, and 4EY6_donepezil exhibited a stable trend with minimal fluctuations around 300 K throughout the 50-nanosecond simulation, indicating proper temperature coupling and stable thermal conditions. The pressure plot (Figure 16B) shows significant fluctuations between −400 bar and 400 bar for all complexes. The density plot for all complexes exhibits a similar trend to the temperature plot, which remains stable around 1044 kg/m^3 throughout the 50-nanosecond simulation (Figure 16C). Overall, the results indicate that the system remains stable throughout the 50-nanosecond simulations, with a slight fluctuation in pressure.

In conclusion, based on the MD results, 4EY6_AL20E exhibits the highest stability, as well as higher hydrogen bond counts and compactness, with reduced flexibility and optimal energy levels, reaffirming its effectiveness as an AChE inhibitor.

4. Conclusion

This study investigated the potential of alkaloids from the marine red seaweed *J. rubens* as inhibitors of human AChE, a key target for treating neurodegenerative diseases, such as AD. Using *in silico* methods, including molecular docking, MD, and DFT studies, we identified seven novel analogs of ursodeoxycholic acid (AL20A–AL20G). Among these, the AL20E derivative, (4R)-4-([3S,7S,8R,9S,10S,13R,14S,17R]-3,7-dihydroxy-10,13-dimethylhexadecahydro-1H-cyclopenta[a]phenanthren-17-yl)pentanamide, demonstrated superior characteristics. It exhibited a favorable toxicity profile and improved drug-likeness compared to both the parent compound (AL20) and the FDA-approved drug, donepezil. MD simulations confirmed the stability of AL20E's binding, showing three strong HBs with key amino acid residues in the protein's hydrophobic region. The BOILED-Egg model also predicted good GI absorption for AL20E. These findings strongly recommend AL20E as a promising candidate for further research and development as an anti-Alzheimer's drug.

Acknowledgments

The authors wish to appreciate the Royal Society of Chemistry, Computer Laboratory at the D. K. Olukoya Central Research & Reference Laboratories, University of Lagos, for supporting this research.

Funding

None.

Conflict of interest

The authors declare that they have no competing of interests.

Author contributions

Conceptualization: Owoyemi W. Elegbeleye, Luqman A. Adams, Oluwole B. Familoni
Data curation: Oluwafemi S. Aina, Mujeeb O. Rofiu, Nafisat O. Babamusa
Formal analysis: Oluwafemi S. Aina
Investigation: Oluwafemi S. Aina, Luqman A. Adams
Methodology: Oluwafemi S. Aina, Mujeeb O. Rofiu, Nafisat O. Babamusa
Supervision: Luqman A. Adams, Oluwole B. Familoni
Writing–original draft: Oluwafemi S. Aina, Owoyemi W. Elegbeleye
Writing–review & editing: Oluwafemi S. Aina, Kafayat A. Owoseni-Fagbenro, Olubusayo F. Semire, Olasupo A. Idris, Nafisat O. Babamusa, Luqman A. Adams

Ethics approval and consent to participate

Not applicable.

Consent for publication

Not applicable.

Availability of data

All data generated in this study are included in the manuscript.

References

1. Li B, He DJ, Li XJ, Guo XY. Modeling neurodegenerative diseases using non-human primates: Advances and challenges. *Ageing Neurodegener Dis*. 2022;2(3):12.

   doi: 10.20517/and.2022.14

2. Kumar A, Sudevan ST, Nair AS, *et al*. Current and future nano-carrier-based approaches in the treatment of Alzheimer's disease. *Brain Sci*. 2023;13(2):213.

   doi: 10.3390/brainsci13020213

3. Martorana A, Esposito Z, Koch G. Beyond the cholinergic hypothesis: Do current drugs work in Alzheimer's disease? *CNS Neurosci Ther*. 2010;16(4):235-245.

   doi: 10.1111/j.1755-5949.2010.00175.x

4. Joo SS, Won TJ, Lee DI. Potential role of ursodeoxycholic acid in suppression of nuclear factor kappa B in microglial cell line (BV-2). *Arch Pharm Res*. 2004;27(9):954-960.

   doi: 10.1007/bf02975850

5. Giacobini E. Cholinesterase inhibitors: New roles and therapeutic alternatives. *Pharmacol Res*. 2004;50(4):433-440.

   doi: 10.1016/j.phrs.2003.11.017

6. Bores GM, Huger FP, Petko W, *et al*. Pharmacological evaluation of novel Alzheimer's disease therapeutics: Acetylcholinesterase inhibitors related to galanthamine. *J Pharmacol Exp Ther*. 1996;277(2):728-738.

7. Cortez LM, Campeau J, Norman G, *et al*. Bile acids reduce prion conversion, reduce neuronal loss, and prolong male survival in models of prion disease. *J Virol.* 2015;89(15): 7660-7672.

   doi: 10.1128/JVI.01165-15

8. Silva RF, Rodrigues CM, Brites D. Bilirubin-induced apoptosis in cultured rat neural cells is aggravated by chenodeoxycholic acid but prevented by ursodeoxycholic acid. *J Hepatol.* 2001;34(3):402-408.

   doi: 10.1016/S0168-8278(01)00015-0

9. Guven KC, Percot A, Sezik E. Alkaloids in marine algae. *Mar Drugs*. 2010;8(2):269-284.

   doi: 10.3390/md8020269

10. Souza CR, Bezerra WP, Souto JT. Marine alkaloids with anti-inflammatory activity: Current knowledge and future perspectives. *Mar Drugs*. 2020;18(3):147.

    doi: 10.3390/md18030147

11. El-Din SMM, El-Ahwany AM. Bioactivity and phytochemical constituents of marine red seaweeds (*Jania rubens*, *Corallina mediterranea* and *Pterocladia capillacea*). *J Taibah Univ Sci*. 2016;10(4):471–484.

    doi: 10.1016/j.jtusci.2015.06.004

12. Trott O, Olson AJ. AutoDock Vina: Improving the speed and accuracy of docking with a new scoring function, efficient optimization, and multithreading. *J Comput Chem*. 2010;31(2):455-461.

    doi: 10.1002/jcc.21334

13. Morris GM, Goodsell DS, Halliday RS, *et al*. Automated docking using a Lamarckian genetic algorithm and an empirical binding free energy function. *J Comput Chem*. 1998;19(14):1639-1662.

    doi: 10.1002/(sici)1096-987x(19981115)19:14%3c1639:aid-jcc10%3e3.0.co;2-b

14. Lipinski B, Herzog H, Kops ER, Oberschelp W, Müller-Gärtner HW. Expectation maximization reconstruction of positron emission tomography images using anatomical magnetic resonance information. *IEEE Trans Med Imaging*. 1997;16(2):129-136.

    doi: 10.1109/42.563658

15. Frisch MJ, Trucks GW, Schlegel HB, *et al*. *Gaussian 09, Revision B.01*. Connecticut: Gaussian Inc., 2010. Available from: https://cir.nii.ac.jp/crid/1370298757422456580 [Last accessed on 2023 Mar 12].

16. Rivero P, Moreira IDP, Illas F, Scuseria GE. Reliability of range-separated hybrid functionals for describing magnetic coupling in molecular systems. *J Chem Phys*. 2008;129(18):184110.

    doi: 10.1063/1.3006419

17. Bielecki J, Lipiec E. Basis set dependence using DFT/B3LYP calculations to model the Raman spectrum of thymine. *J Bioinform Comput Biol*. 2016;14(1):1650002.

    doi: 10.1142/s0219720016500025

18. García-Valverde M, Cordero NA, De la Cal ES. Gaussview (R) as a tool for learning organic chemistry. In: *Edulearn15: 7th International Conference on Education and New Learning Technologies*; 2015. p. 4366-4370.

19. Chitra L, Kumar CR, Basha HM, Ponne S, Boopathy R. Interaction of metal chelators with different molecular forms of acetylcholinesterase and its significance in Alzheimer's disease treatment. *Proteins*. 2013;81(7):1179-1191.

    doi: 10.1002/prot.24267

20. Murugesan B, Somasundram B, Samykannu G, *et al*. Exploring lichen-derived compounds as potential anti-cervical cancer agents: An DFT and MD simulation analysis. *In-Silico Pharmacol*. 2025;13(2):114.

    doi: 10.1007/s40203-025-00380-y

21. Daina A, Zoete V. A BOILED-Egg to predict gastrointestinal absorption and brain penetration of small molecules.

ChemMedChem. 2016;11(11):1117-1121.

doi: 10.1002/cmdc.201600182

22. Daina A, Michielin O, Zoete V. iLOGP: A simple, robust, and efficient description of n-octanol/water partition coefficient for drug design using the GB/SA approach. *J Chem Inf Model*. 2014;54(12):3284-3301.

doi: 10.1021/ci500467k

23. Lipinski CA, Lombardo F, Dominy BW, Feeney PJ. Experimental and computational approaches to estimate solubility and permeability in drug discovery and development settings. *Adv Drug Deliv Rev*. 2001;46(1):3-26.

doi: 10.1016/S0169-409X(00)00129-0

24. Pardridge WM. The blood-brain barrier: Bottleneck in brain drug development. *Neurotherapeutics*. 2005;2(1):3-14.

doi: 10.1602/neurorx.2.1.3

25. Barthe L, Woodley J, Houin G. Gastrointestinal absorption of drugs: Methods and studies. *Fundam Clin Pharmacol.* 1999;13(2):154-168.

doi: 10.1111/j.1472-8206.1999.tb00334.x

26. Mollazadeh S, Sahebkar A, Hadizadeh F, Behravan J, Arabzadeh S. Structural and functional aspects of P-glycoprotein and its inhibitors. *Life Sci.* 2018;214:118-123.

doi: 10.1016/j.lfs.2018.10.048

27. Lin JH, Yamazaki M. Role of P-glycoprotein in pharmacokinetics: Clinical implications. *Clin Pharmacokinet.* 2003;42(1):59-98.

doi: 10.2165/00003088-200342010-00003

28. Dong J, Qin Z, Zhang WD, *et al*. Medicinal chemistry strategies to discover P-glycoprotein inhibitors: An update. *Drug Resist Update.* 2020;49:100681.

doi: 10.1016/j.drup.2020.100681

29. Aina OS, Rofiu MO, Oloba-Whenu OA, Olasupo IA, Adams LA, Familoni OB. Drug design and *in-silico* study of 2-alkoxylated quinoline-3-carbaldehyde compounds: Inhibitors of *Mycobacterium tuberculosis*. *Sci Afr.* 2024;23:e01985.

doi: 10.1016/j.sciaf.2023.e01985

30. Geerlings P, Chamorro E, Chattaraj PK, *et al*. Conceptual density functional theory: Status, prospects, issues. *Theor Chem Acc*. 2020;139(2):36.

doi: 10.1007/s00214-020-2546-7

31. Pal R, Chattaraj PK. Electrophilicity index revisited. *J Comput Chem*. 2023;44(3):278-297.

doi: 10.1002/jcc.26886

32. Galabov B, Ilieva S, Koleva G, Allen WD, Schaefer HF 3rd, Schleyer PVR. Structure-reactivity relationships for aromatic molecules: Electrostatic potentials at nuclei and electrophile affinity indices. *Wiley Interdiscip Rev Comput Mol Sci*. 2013;3(1):37-55.

doi: 10.1002/wcms.1112

33. Dos Santos MAB, De Oliveira LFS, De Figueiredo AF, *et al.* Molecular electrostatic potential and chemometric techniques as tools to design bioactive compounds. *In: Cheminformatics and its Applications*. London: IntechOpen; 2019.

doi: 10.5772/intechopen.89113

34. Berendsen HJC, Van der Spoel D, Van Drunen R. GROMACS: A message-passing parallel molecular dynamics implementation. *Comput Phys Commun*. 1995;91(1-3):43-56.

doi: 10.1016/0010-4655(95)00042-e

35. Shintani EY, Uchida KM. Donepezil: An anticholinesterase inhibitor for Alzheimer's disease. *Am J Health Syst Pharm*. 1997;54(24):2805-2810.

doi: 10.1093/ajhp/54.24.2805